Macromolecules
ARTICLE

*Macromolecules* **2010**, *43*, 4871–4878 **4871**
DOI: 10.1021/ma1004259

# Impact of Initiator Spacer Length on Grafting Polystyrene from Silica Nanoparticles

**Daniel Sunday, Sara Curras-Medina, and David L. Green***

*Department of Chemical Engineering, University of Virginia, 102 Engineers Way, Charlottesville, Virginia 22904*

*Received July 9, 2009; Revised Manuscript Received April 14, 2010*

ABSTRACT: Using atom transfer radical polymerization (ATRP), we synthesized hybrid organic/inorganic nanoparticles consisting of a silica core and a polystyrene brush. The brushes were grafted from the nanoparticles with three different initiators, termed 3-BIDS, 11-BIDS, and 15-BIDS, consisting respectively of a 3-, 11-, or 15-carbon spacer separating an ethoxylated silane from a brominated initiator end group. The initiators were characterized using $^{1}$H NMR and $^{13}$C NMR. Surface modification studies with all three initiators were performed to optimize their attachment, producing particles with dense covalently attached initiator monolayers with up to 2.6 initiators/nm$^2$. Polymers were then grafted from the particles using ATRP, the polymerization kinetics were characterized using gas chromatography (GC), and the final products were characterized using thermogravimetric analysis (TGA) and gel permeation chromatography (GPC). Analysis of the kinetics show an approximately identical rate of styrene conversion from all three initiators while GPC results show that the molecular weight of the polymers grown from the 11-BIDS monolayer increases faster than that grown from 3-BIDS or 15-BIDS. We also found that the graft densities of polystyrene are on average 0.5 chains/nm$^2$ greater for particles modified with 3-BIDS or 15-BIDS at 0.7 chains/nm$^2$ than for 11-BIDS at 0.2 chains/nm$^2$. Our results indicate that the roughly 3-fold drop in graft density for the particles modified with the 11-BIDS is most likely due to a change in the conformation of the 11-BIDS monolayer.

## 1. Introduction

Our objective is to attach alkoxysilane initiators to the surface of silica nanoparticles and quantify the impact of the carbon spacer length (CSL) of the initiator on grafting polystyrene from nanoparticle surfaces. Over the past decade investigators have shown that "grafting from" reactions permit the attachment of dense polystyrene brushes or polystyrene polymers end-tethered to surfaces. Our study addresses the paucity of research in evaluating the impact of the CSL of the covalently attached initiator monolayer on the monomer-by-monomer polymerization from surfaces. These types of studies are important, as surface modifications through controlled/living polymerizations have become versatile and powerful techniques for developing advanced materials. In particular, initiating polymer synthesis from surfaces rather than attaching a preformed polymers to surfaces produces much higher graft densities while maintaining excellent control over polymer architecture.[1−4] Materials synthesized by grafting polymers from surfaces have been used in a wide variety of applications including colloidal stability,[5] control of bacteria and protein adhesion,[6,7] drug delivery,[8] lubrication,[9,10] and mechanical reinforcement.[11,12] In addition, "grafting from" reactions have been carried out from a wide range of materials including gold,[13,14] clay,[1] carbon particles,[15] iron oxides,[16,17] carbon nanotubes,[18] and most predominantly silica nanoparticles[2−4,7,19−24] and silicon wafers.[7,13,25,26]

Although a variety of controlled/living polymerization methods exist, atom transfer radical polymerization (ATRP) is currently the most popular. This is due to both its ease of use and its versatility in the combinations of monomer, initiator, solvent, and catalyst employed to produce the desired products.[22,27−30] ATRP is a controlled/living polymerization in which chain growth is governed via cycles of activation and deactivation.[31] Chain growth is activated by the abstraction of a halogen by a transition metal−ligand catalyst, and growth is deactivated by the return of the halogen to the chain through the reduction of the catalyst. Accordingly, the concentration of active chains controls the polymerization rate, which is proportional to the ratio of the oxidation states of the metal species (e.g., [Cu(I)]/[Cu(II)]).[3,27,32] This reaction chemistry also applies to surface-initiated ATRP (SI-ATRP), which first requires the attachment of an initiator with a halogen end group from which polymerization occurs. Initiators can be assembled from the surface[20] or synthesized separately and subsequently attached. Specifically for silica, most initiators consist of a silane coupling agent and an ATRP initiator group connected via a carbon chain whose number of methylene groups define the carbon spacer length (CSL).[4]

While surveying the literature it can be seen that initiators of varying CSL have been used in the SI-ATRP of polymers from silica;[3,7,22,33] however, no study has been performed to shed light on the impact of the initiator CSL on grafting polymers from surfaces. Typically, increasing the CSL of the self-assembled monolayer (SAM) mitigates nanoparticle aggregation by preventing the close contact of nanoparticle surfaces and prevents the undesirable adsorption of polymers to both flat surfaces and nanoparticles.[34,35] Thus, the SAM can prevent uncontrolled particle aggregation and polymer adsorption both of which have been shown to erode the properties of advanced materials such as polymer nanocomposites.[36,37] Toward this end, initiators with a CSL of three are the most commonly used throughout the literature, with most of the studies being performed from particles,[2−4,15,17,20,23,24,38−40] although the 3 CSL initiator

*Corresponding author. E-mail: dlgreen@virginia.edu.



Published on Web 05/07/2010

has been used to graft polymers from flat surfaces.[41] In contrast, 11 CSL initiators are used more sparingly and almost exclusively on flat surfaces.[13,25,33,42,43] To our knowledge, the longest CSL used in an initiator was 16 and was attached to both particles and flat surfaces.[7] To date, no study has been performed to determine the impact of the carbon spacer length (CSL) of the alkoxysilane initiator on grafting polystyrene from silica nanoparticles.

Thus, to compare results between polystyrene chains grown from initiators of different sizes, three initiators with CSL's of 3, 11, and 15 were synthesized and attached to the surface of monodisperse silica nanoparticles. The 3 CSL initiator—3-(2-bromoisobutyryl)propyl)dimethylethoxysilane (3-BIDS)—and the 11 CSL initiator—11-(2-bromoisobutyryl)undecyldimethylethoxysilane (11-BIDS)—were synthesized previously,[4,42] while the 15 CSL initiator—15-(2-bromoisobutyryl)pentadecyl)dimethylethoxysilane (15-BIDS)—is a new molecule from this research. Polystyrene was subsequently grafted from silica nanoparticle surfaces, and specific attention was placed on elucidating how the initiator CSL affects the SI-ATRP of polystyrene as quantified by its graft density ($\Sigma$), graft polymer molecular weights ($M_n$), and polydispersities (PDI). Overall, the knowledge gained from quantifying the effect of the initiator CSL on grafting polystyrene from nanoparticle surfaces can then be used to tailor the properties of advanced materials for various applications.

## 2. Experimental Methodology

**2.1. Materials.** Ethanol, methanol, and dichloromethane were purchased from Mallinckrodt. Methyl ethyl ketone (MEK), methyl isobutyl ketone (MIBK), diethyl ether, hexane, ethyl acetate, and triethylamine were purchased from Fisher Scientific. Styrene, also purchased from Fisher, was filtered through a column of basic alumina to remove the inhibitor. The reagents $\omega$-pentadecalactone, *n*-bromosuccinimide, and triphenylphosphine were purchased from Sigma-Aldrich. Karstedt's catalyst and dimethylethoxysilane were purchased from Gelest. All other chemicals were purchased from Acros and used as received.

**2.2. Synthesis.** Uniform, monodisperse silica nanoparticles with radius $R \approx 25$ nm were synthesized via the Stöber method[44,45] with [TEOS] = 0.5 M, [$H_2O$] = 1.07 M, and [$NH_3$] = 0.45 M in ethanol. TEOS is an abbreviation for tetraethyl orthosilicate. Subsequently, ATRP initiators were attached the surface of the silica nanoparticles where the 3-BIDS[4] and 11-BIDS[42] were synthesized according to literature procedures. The initiator 15-(2-bromoisobutyryl)pentadecyl)dimethylethoxysilane (15-BIDS) was synthesized through the esterification of pentadec-14-en-1-ol[46] with 2-bromomethylpropionyl bromide, resulting in the product pentadec-14-enyl-2-bromo-2-methylpropanoate, followed by its hydrosilylation with dimethylethoxysilane. SI-ATRP of polystyrene was subsequently carried out from the surface of the functionalized silica nanoparticles.

*2.2.1. Synthesis of Pentadec-14-enyl-2-bromo-2-methylpropanoate.* 14-Pentadec-en-1-ol (1 g, 0.004 mol) was dissolved in 20 mL of dichloromethane along with triethylamine (3 mL, 0.0041 mol). The solution was cooled to 0 °C in an ice bath, and 2-bromomethylpropionyl bromide (1.15 mL, 0.0035 mol) was added dropwise. The solution was warmed to room temperature and reacted for 24 h. The products were washed three times with 20 mL of deionized water, and the organic layer was dried over $MgSO_4$. Solids were filtered out, and the solvent was removed under reduced pressure at 90 °C. 1.15 g of the final product was obtained for a 77% yield. $^1$H NMR (300 MHz, $CDCl_4$): 1.25−1.4 (m, 20H), 1.71 (m, 2H), 1.96 (S, 6H) 2.1 (m, 2H), 4.2 (t, $J$ = 7 Hz, 2H), 4.90 (d, $J$ = 10.2 Hz, 1H), 4.99 (d, $J$ = 18.4 Hz, 1H), 5.81 (ddt, $J$ = 17, 10.5, 6.6 Hz, 1H). $^{13}$C NMR (300 MHz, $CDCl_4$) (ppm): 26, 28.6, 29.2, 29.4, 29.7−29.9, 31, 56, 66, 115, 139, 172.

*2.2.2. Synthesis of 15-(2-Bromoisobutyryl)pentadecyl)dimethylethoxysilane (15-BIDS).* Pentadec-14-enyl-2-bromo-2-methylpropanoate (3.38 g, 0.009 mol) was added to a round-bottom flask along with dimethylethoxysilane (1.63 mL, 0.011 mol), and subsequently Karstedt's catalyst (0.01 mL) was added. The solution was heated at reflux for 8 h, and then unreacted dimethylethoxysilane was evaporated under reduced pressure. The product was filtered through a short column of silica gel to remove the catalyst. 3.54 g of the final product was obtained with a 85% yield. $^1$H NMR (300 MHz, $CDCl_4$): 0.1 (m, 6H), 0.55 (m, 2H), 1.2−1.37 (m, 20H), 1.71 (m, 2H), 1.96 (S, 6H) 2.1 (m, 2H), 3.79, (q, 2H), 4.2 (t, 2H). $^{13}$C NMR (300 MHz, $CDCl_4$) (ppm): 0.6, 18, 23.5, 26, 29.6−29.9, 31, 33, 55, 66, 101, 172.

*2.2.3. Functionalization of Silica Nanoparticles.* The procedure for attachment of the 3-BIDS, 11-BIDS, and 15-BIDS initiators to the surface of the silica nanoparticles was identical. A representative example is shown below. First, 188 mL of $SiO_2$ (15 wt %) in methyl isobutyl ketone (MIBK) or methyl ethyl ketone (MEK) was added to a round-bottom flask along with 26.2 g of the initiator (0.088 mol). The solution was heated at reflux for 24 h; afterward, the excess initiator was removed through five cycles of centrifugation and resuspension in hexane. Excess solvent was removed under vacuum.

*2.2.4. SI-ATRP of Styrene from Functionalized Silica Nanoparticles.* The procedure to graft polystyrene from the surface of the silica nanoparticles was identical for those modified with the 3-BIDS, 11-BIDS, and 15-BIDS initiators. The functionalized nanoparticles (0.75 g) were placed in a Schlenk flask along with styrene (10 mL, 0.087 mol) and anisole (8.3 mL, 0.0929 mol). The flask was then capped with a septum and degassed through at least three freeze/thaw cycles. The flask was subsequently transferred into a glovebox under nitrogen, and the septum was removed, facilitating the addition of the transition metal−ligand catalyst, CuBr(I)/PMDETA (1.7 mL of a 15 mg/mL solution in anisole, 1:1 molar ratio of CuBr(I):PMDETA), to the flask, followed by the replacement of the septum. The Schlenk flask with its contents was then placed into a 90 °C oil bath, and aliquots were taken and analyzed periodically to quantify their reaction kinetics. Subsequently, the styrene-grafted silica nanoparticles (PS-*g*-silica) were separated from the free polymer by diluting the remaining reaction mixture with THF and centrifuging the product. The free polymer was removed in the supernatant, and the particles were redispered in THF. This cycle was repeated until no polymer was visible upon precipitation of the supernatant in methanol. Upon successful removal of the free polymer, the particles in THF were precipitated into methanol to remove the copper. The solids were recovered via filtration, and this process was repeated until the particles were white in color, which were then dried under vacuum.

Prior to characterization, the PS graft polymer was etched from the silica nanoparticles with hydrofluoric acid (HF). Etching was accomplished by adding to a plastic vial the PS-*g*-silica particles (250 mg), toluene (10 mL), phase transfer catalyst Aliquot 336 (75 mg), and a 2% aqueous solution of HF (15 mL), sealing the vial and shaking the contents. Etching was allowed to take place for several hours, at which point the shaking was stopped and the aqueous and organic phases were allowed to separate. The organic phase was then removed and washed with a saturated sodium bicarbonate solution to neutralize residual HF, and the graft polymer was precipitated in methanol and prepared for analysis.

**2.3. Characterization.** A JEOL 6700F field emission scanning electron microscope (SEM) was used to determine the geometric size of the silica nanoparticles. A portion of the aliquots, whose collection was discussed in the previous section, were analyzed gas chromatrography (GC) to quantify the conversion of styrene with respect to time as measured with a Shimadzu GC 2010 with an AOC-20s autosampler, a Shimadzu Shim5 column, and

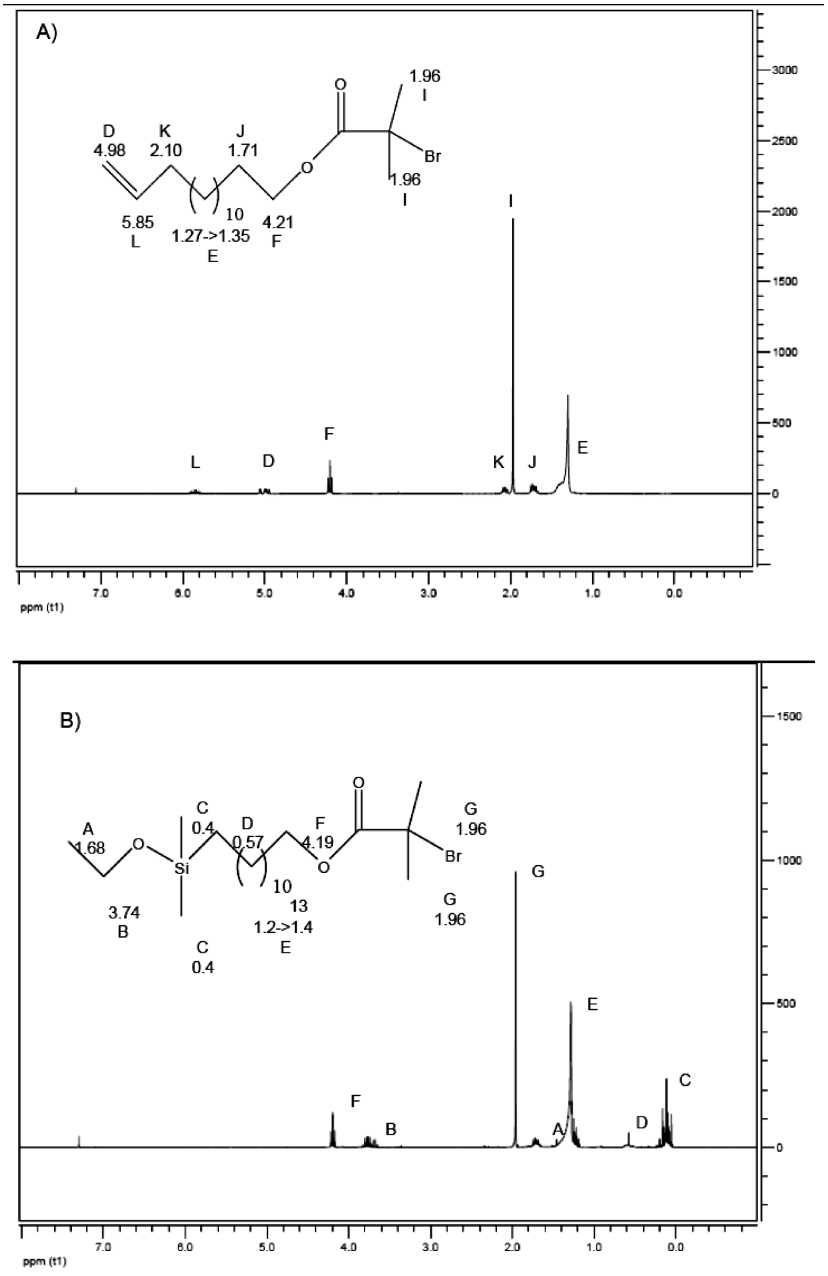


**Figure 1.** $^{1}$H NMR scans of (A) pentadec-14-enyl-2-bromo-2-methylpropanoate, the precursor to 15-BIDS, and (B) 15-BIDS.

a flame ionization detector. Helium was used as the carrier gas at a flow rate of 2.44 mL/min, and the temperature was ramped from $T$ = 60 to 160 at 5 °C/min. The graft polymers were separated from the silica particles as described in the previous section, and gel permeation chromatography (GPC) was used to determine the number-average molecular weights ($M_n$) of the graft polymers and their polydispersities (PDI = $M_n/M_w$), where $M_w$ is the weight-average molecular weight. Polystyrene standards were used to calibrate the GPC on a Hewlett-Packard instrument (series 1100 HPLC) equipped with Polymer Laboratories 5 mm mixed-C columns and connected to UV−vis and refractive index detectors. THF was used as the diluent for the samples at a temperature of 20 °C and flow rate of 1.0 mL/min. GPC data were analyzed with OmniSEC software. $^{1}$H and $^{13}$C NMR spectra were collected on a Varian 300 MHz spectrometer and analyzed with MestRec software.

To determine the initiator and graft polymer densities, thermogravimetric analysis (TGA) was performed on a TA Instruments SDT Q600, using a temperature ramp rate of 10 °C/min up to 1000 C. Samples were kept under vacuum for at least 12 h prior to analysis. The initiator surface coverage ($\sigma_i$) was calculated from TGA using eqs 1a−1d.

$$M_S = \frac{(W_m - W_{um})M_I}{1 - W_{um}} \tag{1a}$$

$$M_{SiO_2} = M_I - M_S \tag{1b}$$

$$A_S = \frac{3M_{SiO_2}}{R\rho_{SiO_2}} \tag{1c}$$

$$\sigma_i = \frac{M_S N_A}{M_w A_S} \tag{1d}$$

TGA was used to determine $\sigma_i$ by first quantifying mass of the initiator on the particle surface, $M_s$, from difference in the

percentages of total weight lost between modified and unmodified particles, or $W_m$ and $W_{um}$, respectively, where $M_I$ is the mass of the modified particles prior to TGA in eq 1. To account for the loss of volatile compounds which were not covalently bonded to the particles, the mass at 250 °C was taken as the initial weight, and 800 °C was taken as the final weight. Representative TGA curves are shown in the Supporting Information. Subsequently, $\sigma_i$ was calculated in eq 1d from the surface area of the bare silica nanoparticles, $A_s$, in eq 1c, where $M_{SiO_2}$, $\rho_{SiO_2}$, and $R$ are the mass, mass density, and geometric size, respectively, of the unmodified nanoparticles. Moreover, $N_A$ is the Avogadro number, and $M_w$ is the molecular weight of the initiator on the surface. Equations 1a−1d are also used to calculate the polystyrene graft density, Σ, where it is substituted for $\sigma_i$ in eq 1d, whereas $W_m$ and $M_I$ are for the PS-*g*-silica nanoparticles and $M_w$ is the molecular weight of a styrene monomer.

A dynamic light scattering apparatus (DLS) from PhotoCor Instruments was used to determine the hydrodynamic radius ($R_h$) of the unmodified, initiator modified, and polystyrene-grafted nanoparticles. The DLS consists of a helium−neon laser, sample holder, and photodetector. The hydrodynamic radii of the particles were calculated from photon−photon autocorrelation functions, from which particle diffusion coefficients ($D_e$) were determined using a third-order cumulant analysis. The hydrodynamic radii ($R_h$) were determined from $D_e$ through the Stokes−Einstein relation in eq 2

$$R_h = \frac{k_B T}{6\pi\eta D_e} \tag{2}$$

where $k_b$ is the Boltzmann constant, $T$ the absolute temperature, and $\eta$ the solution viscosity. All measurements were carried out at room temperature in THF.

## 3. Results and Discussion

We investigated how the carbon spacer length (CSL) of the initiator impacts the SI-ATRP of styrene from silica nanoparticles by synthesizing three initiators that vary in CSL, attaching them to the particles, and polymerizing polystyrene from silica. To our knowledge, our study is the first to quantify the impact that initiator CSL can have on grafting polymers from nanoparticle surfaces with ATRP. Accordingly, the "grafting from" reactions of polystyrene from the self-assembled monolayers (SAMs) were carried out under the same reactant concentrations of catalyst ([CuCl] = $9.1 \times 10^{-3}$ M), ligand ([dNbipy] = $1.0 \times 10^{-2}$ M), monomer ([styrene] = 4.31 M), and solvent ([anisole] = 4.60 M). A very small amount of free polymer grew in solution during the reaction, and as discussed in this section, our mass balance calculations from our GC measurements indicate that the free polymer constituted only 0.5% of the total mass of polymerized styrene. Thus, the molecular weight of the free polymer was not quantified as our interest was on surface properties. To this end, the CSL of the initiator was increased 5-fold, from 3−15 methylene units, to determine the impact of CSL of the SAM on the SI-ATRP of polystyrene from silica nanoparticles.

To verify that the initiators were synthesized successfully, both $^1$H NMR and $^{13}$C NMR were used. The $^1$H NMR scan for 15-BIDS and its precursor, pentadec-14-enyl-2-bromo-2-methylpropanoate, are shown in Figure 1. The complete hydrosilylation of the precursor to 15-BIDS occurred when the double bonds, or the allyl peaks of the precursor at 4.98 and 5.85 ppm in Figure 1a, were nonexistent in Figure 1b, indicating that the monoethoxysilane anchoring group was attached to the precursor to form 15-BIDS. Based on Figure 1a,b, the bromine moiety, from which polymerization is initiated, was retained throughout the synthesis. This can be observed from the location of the peaks of the neighboring methyl hydrogen at ~1.97 ppm in Figure 1a,b.

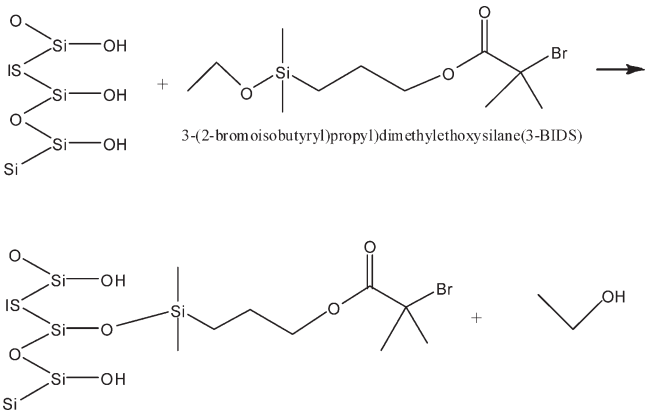


**Figure 2.** Schematic of the surface modification of silica nanoparticles with 3-BIDS initiator.

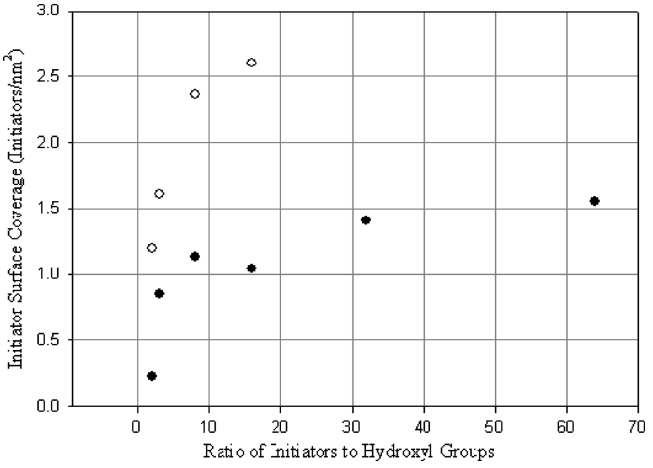


**Figure 3.** Comparison between initiator coverage for 3-BIDS modified in (●) MEK and (○) MIBK.

The syntheses of the 3-BIDS and 11-BIDS initiators were confirmed in a similar fashion. The $^1$H NMR and $^{13}$C NMR results for the 3-BIDS and 11-BIDS are included in the Supporting Information.

Attachment of the SAM is the first step in grafting most polymers from surfaces where Figure 2 shows a schematic of the condensation reaction in which ATRP initiators are attached to silica nanoparticles. To ensure full initiator coverage, which typically improves particle stability and mitigates polymer adsorption, adsorption experiments were performed in which the concentration of initiator in the reaction bath, tracked by the ratio of initiator to hydroxyl groups on the silica surface, was increased until complete monolayer coverage was achieved. Silica has a hydroxyl site density of 5 OH groups/nm$^2$.[47,48]

Full monolayer coverage for the 3-BIDS initiator was benchmarked against the maximum surface coverage for a similar sized monofunctional silane−trimethylethoxysilane (TRMS) on silica at $\sigma_i \approx 2.8$ molecules/nm$^2$.[47,49] Moreover, while the conditions to attach the ATRP initiators were optimized in methyl isobutyl ketone (MIBK), we show the results of the initiator adsorption experiments in both MIBK and methyl ethyl ketone (MEK) in Figure 3 to illustrate the effect of solvent on surface functionalization. The surface coverage of the 3-BIDS initiator in MEK reached a plateau around $\sigma_i \approx 1.6$ initiator/nm$^2$, a value that reflects submonolayer coverage. In contrast, in MIBK, the 3-BIDS initiator reaches $\sigma_i \approx 2.6$ initiators/nm$^2$, reflecting the attainment of a densely packed initiator monolayer. While unmodified silica nanoparticles are electrostatically stable in both

**Table 1. Summary of the Results from All SI-ATRP Reactions of Polystyrene from Silica[a]**

| initiator | time (min) | styrene conv (%) | graft polymer $M_n$ (g/mol) | graft polymer PDI ($M_w/M_n$) | graft density $\Sigma$ (chains/nm$^2$) | initiation efficiency ($\Sigma/\sigma_i$) |
|---|---|---|---|---|---|---|
| 3-BIDS | 120 | 6.9 | 10 900 | 1.24 | 0.73 | 0.28 |
| | 180 | 8.4 | 9 900 | 1.22 | 0.67 | 0.26 |
| | 240 | 12.1 | 14 400 | 1.26 | 0.71 | 0.27 |
| | 320 | 22.1 | 36 100 | 1.20 | 0.77 | 0.30 |
| 11-BIDS | 60 | 1.2 | 9 700 | 1.29 | 0.15 | 0.07 |
| | 120 | 6.5 | 28 400 | 1.31 | 0.2 | 0.09 |
| | 180 | 9.1 | 24 500 | 1.21 | 0.34 | 0.16 |
| | 240 | 10.3 | 40 700 | 1.27 | 0.23 | 0.11 |
| | 300 | 25.1 | 88 800 | 1.37 | 0.2 | 0.09 |
| 15-BIDS | 240 | 10.4 | 16 700 | 1.26 | 0.75 | 0.35 |
| | 180 | 13.9 | 24 500 | 1.21 | 0.75 | 0.35 |
| | 300 | 21.1 | 40 200 | 1.38 | 0.61 | 0.29 |

[a]Average values are reported, and standard deviations, not shown for the sake of clarity, were within 5% of the average based on a 95% confidence interval.

MIBK and MEK, we speculate that higher initiator coverages were obtained in MIBK as it is a less polar solvent, which should reduce its affinity for the silica surface as reflected in its lower dielectric constant ($\varepsilon_{MIBK} \approx 13$, $\varepsilon_{MEK} \approx 18$). In addition, the condensation reaction in MIBK is conducted at a higher reflux temperature, which corresponds to its higher boiling point ($T_{MIBK} = 118$ °C, $T_{MEK} = 80$ °C). Similar experiments were performed in MIBK with 11-BIDS and 15-BIDS, both yielding a lower coverage of $\sigma_i = 2.1$ initiator/nm$^2$, reflecting that the molecules are larger and occupy more space than 3-BIDS. Ultimately, we observed that the nanoparticles functionalized with the 3-BIDS, 11-BIDS, and 15-BIDS initiators were all stable in anisole over a 24 h period, indicating that the particles should remain suspended during the SI-ATRP reactions.

Table 1 gives a complete summary of the SI-ATRP reactions including the percent conversion of styrene as well as the properties of the polystyrene graft layers, including their number-averaged molecular weights ($M_n$), polydispersity indices (PDI = $M_n/M_w$), graft densities ($\Sigma$), and initiation efficiencies ($\Sigma/\sigma_i$) as a function of time and initiator CSL. Figure 4 shows the kinetics for the conversion of styrene as a function of initiator CSL, where the result for all reactions are shown, illustrating the repeatability of the experiments, which were run a minimum three times. Overall, the linearity of the plot of $\ln([M]_0/[M]_t)$ versus time ($t$) indicates that the conversion of styrene is first-order, a characteristic of a controlled polymerization, which has been observed for the SI-ATRP of polystyrene from silica.[3,4] This result indicates that the polymerization kinetics are well controlled in the absence of both free initiator and added deactivator, which are required under some conditions.[4,41] But of greater interest was the overlap of the styrene conversions with time, indicating that the overall rate of polymerization was similar across the 3-BIDS, 11-BIDS, and 15-BIDS initiator monolayers. Ultimately, all reactions were terminated just prior to 30% conversion before the contents in the reaction bath solidified. Solidification has also been observed in other studies in which polystyrene has been grafted from silica with SI-ATRP.[38]

While Figure 4 shows the semilogarithmic conversion of styrene from solution as a function of time, Figures 5 and 6 show respectively the polystyrene graft polymer number-average molecular weight ($M_n$) and the polystyrene graft density ($\Sigma$) as a function of conversion. The $M_n$ of the graft polymer in Figure 5 increase linearly with conversion for all initiator functionalized nanoparticles, which is also indicative of controlled/living polymerization. The polystyrene grafts initiated from 3-BIDS and 15-BIDS monolayers grow at essentially the same rate based on the overlap of their polymer molecular weights. However, the graft polymer molecular weights from the 11-BIDS initiator are considerably higher (2−4 times) than those from the 3-BIDS and 15-BIDS initiators. The controlled nature of the growth of

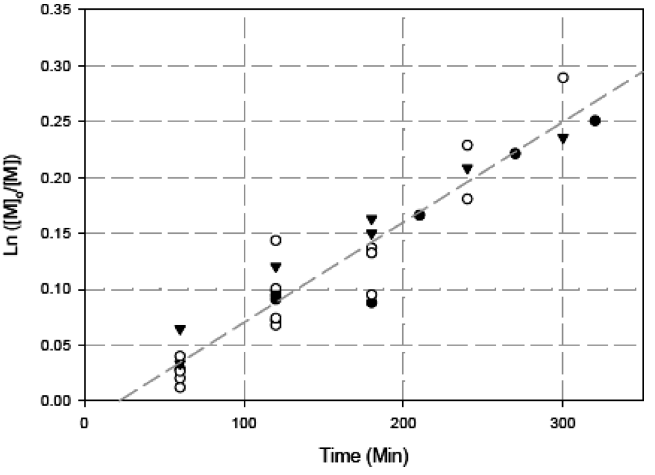


**Figure 4.** Semilogarithmic plot of styrene monomer conversion from silica nanoparticles with all three initiator monolayers (●, 3-BIDS; ○, 11-BIDS; ▼, 15-BIDS). Reactions proceeded at 90 °C with the following reactant conditions: 0.75 g of initiator-modified particles, 10 mL of styrene, 10 mL of anisole, 0.181 mmol of Cu(I)Br, 0.2 mmol of PMDETA. The line represents a fit to 3-BIDS data from the rate constant of 3-BIDS in Table 2. Fits of the rate constants of 11-BIDS and 15-BIDS, not shown for the sake of clarity, are similar to those of 3-BIDS.

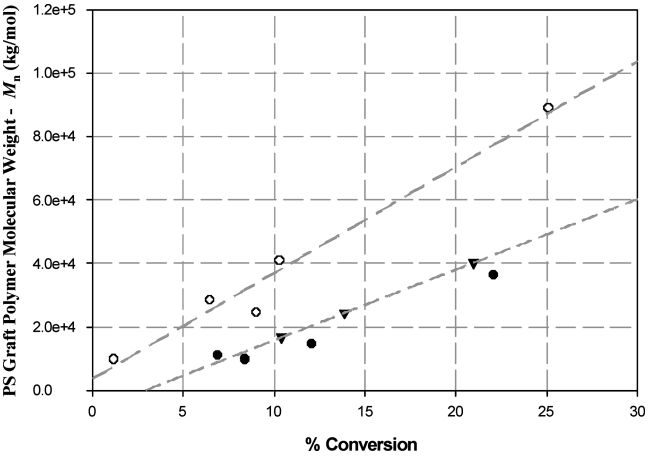


**Figure 5.** Polystyrene graft polymer molecular weight ($M_n$) versus percent styrene conversion for silica nanoparticles modified with initiator monolayers (●, 3-BIDS; ○, 11-BIDS; ▼, 15-BIDS). Lines drawn to aid viewing.

the polystyrene graft layers is further exemplified when examining the change in particle size with conversion (seen in the Supporting Information), demonstrating that the increase in

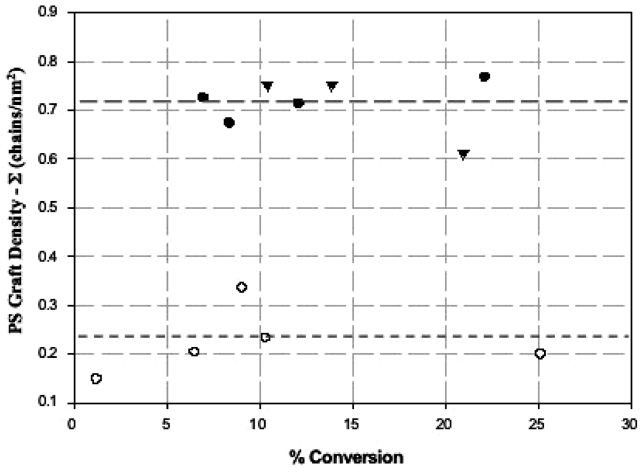


**Figure 6.** Graft density (Σ) of PS polymers versus the percent conversion of styrene for silica nanoparticles modified with initiator monolayers (●, 3-BIDS; ○, 11-BIDS; ▼, 15-BIDS). Lines represent the average of the polystyrene graft density ($\Sigma_{avg}$) for the 15-BIDS and 3-BIDS (long dashes) and 11-BIDS (short dashes).

the hydrodynamic radii of the PS-*g*-silica nanoparticles is essentially linear with $M_n$ during the SI-ATRP reactions.

The impact of the initiator carbon spacer length (CSL) on the SI-ATRP of polystyrene is further illustrated in when comparing the polystyrene graft densities (Σ) with respect to styrene conversion in Figure 6. The reactions from the shortest and longest SAMs, i.e., 3-BIDS and 15-BIDS, both yield high $\Sigma \approx 0.7-0.8$ chains/nm$^2$, which approach the maximum coverage predicted for vinyl monomers such as polystyrene.[50] In contrast, the polystyrene graft densities from the intermediate CSL initiator (11-BIDS) are much lower ($\Sigma \approx 0.15-0.32$ chains/nm$^2$), indicating reduced initiation efficiencies from the 11-CSL monolayers.

These findings show that stark differences in the properties of the polystyrene graft layers result from changing the initiator from either 3-BIDS or 15-BIDS to 11-BIDS, indicating that the CSL of the initiator does affect the SI-ATRP of polystyrene from silica. Using either the longest or shortest spacer length studied here allows the formation of a polymer brush with extremely high graft densities and higher initiation efficiency. The 11-BIDS monolayer appears to offer a method for limiting the graft density of the growing chains while still achieving monolayer coverage around the particle surface. We propose that the decrease in graft density and initiator efficiency for polymers grown from the 11-BIDS initiator most likely stems from changes in the conformation within the monolayer which impacts the accessibility of the terminal Br from which SI-ATRP of polystyrene is initiated.

Figure 7 shows the proposed orientations of the terminal Br of the tertiary α-bromoester of the initiator. On the basis of an all-trans arrangement of the $CH_2$ units of alkyl spacers of the 3-BIDS and 15-BIDS initiators in Figure 7a, we propose that the terminal $C_2$-$(CH_3)_2$Br moiety would be parallel to the surface normal so that both the two $CH_3$ groups and the Br atom would reside in a plane parallel to the particle surface. This would enable high polystyrene graft densities as the Br atom would be equally accessible for atom transfer in solution regardless of its rotation around the terminal carbon of the initiator. Similar conformations have been detected for alkanethiols monolayers on metal surfaces where the orientation of the terminal $CH_3$ group, which depends on the alkyl chain length, impacts reactivity and physical properties of the monolayers.[51,52]

In contrast, we propose that the terminal $C_2$-$(CH_3)_2$Br moiety of the 11-BIDS initiator in Figure 7b tilts from the surface normal, restricting access of the terminal Br for atom transfer. In particular, surface-enhanced Raman scattering studies show

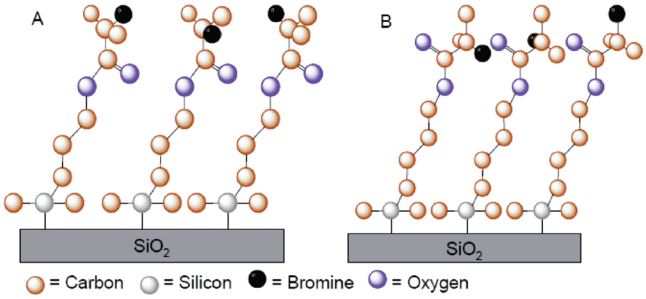


**Figure 7.** Illustration the proposed differences in orientation of the terminal $C_2$-$(CH_3)_2$Br moiety within the (a) 3-BIDS and 15-BIDS monolayers where the terminal moiety would be parallel to the surface normal, enabling terminal Br to be accessible for atom transfer in solution, and (b) 11-BIDS monolayer where the terminal moiety is tilted away from the surface normal, enabling the Br atom to be accessible to atom transfer in proportion to its 1/3 probability of pointing upward to the solution, or in proportion to its rotation about the terminal carbon atom.

that alkanethiol monolayers with 11 carbons exhibit distinctly different behaviors from chains of other lengths based on the presence of gauche conformations in the 11-carbon chain in addition to trans conformations.[53,54] In contrast, alkanethiol monolayers of other chain lengths only display trans conformations.[53,54] Further, the Raman spectra for the alkanethiol monolayer with 11 carbons bears a greater resemblance to the spectra of its bulk solution than any other chain length; the bulk solid spectra of the 11-carbon monolayer also shows evidence of gauche conformations which is unique among the molecules studied.[53] It is important to note that these conformations are seen in the region of carbon−carbon bonds,[54] and more generally, trends in chain conformation are largely independent of the binding chemistry (e.g., sulfur and siloxane linkages) and depend more strongly on numbers of carbons in the chain.[53−55] Therefore, we expect the trends in the conformation of the 11-carbon alkanethiol monolayers to carry over to the 11-carbon ATRP initiator in our study. Thus, we anticipate that the presence of gauche conformations in the 11-BIDS monolayers should affect the orientation of the terminal methyl and bromine moieties, which should inhibit access to the terminal Br to atom transfer, resulting in a decrease in polystyrene graft density during SI-ATRP. In particular, in comparison to the 3-BIDS and 15-BIDS initiator monolayers, we would expect that the PS graft density to decrease by roughly 1/3 on the 11-BIDS monolayer based on the 1/3 probability that the Br of the tertiary α-bromoester would be accessible for atom transfer. This supposition is supported by comparing the ratio of the average PS graft densities from the 11-BIDS monolayer at 0.23 chains/nm$^2$ to that of the 3-BIDS and 15-BIDS monolayers at 0.71 chains/nm$^2$. This ratio is essentially 1/3, supporting the change in conformation of the 11-BIDS monolayer.

An explanation for the nearly identical conversions from the three different monolayers can be inferred from the analysis of the kinetics from SI-ATRP reactions. The analysis is straightforward and involves fitting the SI-ATRP rates equations to extract the apparent first-order rate constant ($k_{app}$) as well as determining the relative ratios of Cu(I)/Cu(II) between the reactions that start from the same reactant concentrations, but take place on different initiator monolayers.

Our analysis starts from extracting the apparent first-order rate constant ($k_{app}$), which connects the disappearance of styrene monomer and its concentration in solution [M] to the rate of polymerization ($R_p$) from the surface. The constant, $k_{app}$, can be determined from eq 3.[27,29]

$$R_p = \frac{-d[M]}{dt} = k_{app}[M] = k_p[M][P^\bullet] \qquad (3)$$

**Table 2. Apparent Rate Constants ($k_{app}$) and the Relative Ratios of Cu(I)/Cu(II) for the SI-ATRP from the 3-, 11-, and 15-BIDS Monolayers**

| initiator | $k_{app}$ (1/s) | copper ratio[a] |
|---|---|---|
| 3-BIDS | $8.6 \times 10^{-4} \pm 0.7 \times 10^{-4}$ | 1.00 |
| 11-BIDS | $1.0 \times 10^{-3} \pm 0.1 \times 10^{-3}$ | 3.22 |
| 15-BIDS | $8.0 \times 10^{-4} \pm 0.9 \times 10^{-4}$ | 0.96 |

[a] Copper ratio is the ratio of [Cu(I)]/[Cu(II)] of the 3-BIDS monolayer to that of a given system. The copper ratio is computed from eq 6. This computation is discussed within the text.

Thus, $k_{app}$ is proportional to the rate constant of free radical polymerization ($k_p$) for polystyrene and the concentration of active polystyrene chains that end with free radicals [P$^\bullet$].

The rate constants for $k_{app}$ were calculated by fitting eq 3 to the styrene conversion data in Figure 4. The values for $k_{app}$, presented in Table 2, are statistically the same regardless of the carbon spacer length of the 3-BIDS, 11-BIDS, and 15-BIDS initiator monolayers. Because $k_p$ depends on temperature,[56] it should also remain constant throughout all reactions from the monolayer, which were carried out at a constant temperature $T = 90$ °C. Thus, [P$^\bullet$] must also be approximately constant from reactions on all three monolayers based on the overlap in [M] from Figure 4.

The free radical concentration, [P$^\bullet$], is related to the rates, rate constants, and concentrations of copper species connected to activation ($k_a$ and [Cu(I)]) and deactivation (the deactivation rate constant, $k_d$, and [Cu(II)]) of the polystyrene polymers as well as their concentrations [P−Br] in eq 4.[27,29]

$$[P^\bullet] = \frac{k_a}{k_d}[P-Br]\frac{[Cu^{(I)}]}{[Cu^{(II)}]} \quad (4)$$

$$R_p = \frac{-d[M]}{dt} = k_p\frac{k_a}{k_d}[M][P-Br]\frac{[Cu^{(I)}]}{[Cu^{(II)}]} \quad (5)$$

Substituting eq 4 into eq 3 yields eq 5, which can be further analyzed to quantify how the initiator conformation would affect the polymerization of styrene from the different monolayers. In particular, because the rates of polymerization $R_p$ from the initiator monolayers are statistically equal, it is advantageous to analyze the ratio of the polymerization rates from the different monolayers to infer how the accessibility of the terminal Br for atom transfer would impact the ratio of [Cu(I)]/[Cu(II)].

The polystyrene graft density, Σ, is essentially equal to [P−Br], or the number of growing chains in the reaction, because the polymerization of polystyrene occurs primarily from the particle surface and not in solution. This assertion is supported by comparing the balance of mass from the conversion of styrene from solution to that of styrene on the particle surface. For example, in the case of the first reaction in Table 1, the total mass of polymerized styrene is 0.627 g (found by multiplying the total mass of styrene in the solution by the 6.9% conversion), and the mass of polystyrene on the particle surface is 0.625 g (found by multiplying the total number of chains in the solution by its $M_n$), leaving only ~0.002 g as free polymer or less than 0.5% of the total mass of polymerized styrene. Subsequently, taking the ratios of the $R_p$ between different systems permits the cancellation of the rate constants, $k_a$, $k_d$, and $k_p$ which depend on the reaction conditions, which are the same from the different monolayers.

Thus, substituting the graft density Σ for the number of growing chains [P−Br] and calculating the ratio of the polymerization rates $R_p$ yields

$$\frac{\Sigma_j}{\Sigma_i} = \left(\frac{[Cu(I)/Cu(II)]_i}{[Cu(I)/Cu(II)]_j}\right)\left(\frac{R_{p,j}}{R_{p,i}}\right) \quad (6)$$

where the subscripts $i$ and $j$ represent grafting reactions carried out from different initiator monolayers, e.g., $i$ = 3-BIDS and $j$ = 11-BIDS or 15-BIDS. On the basis of eq 6, a relative change in the graft densities from different monolayers should be accompanied by changes in the relative ratio of Cu(I)/Cu(II). Thus, if the ratio of the polymerization rates ($R_{p,j}/R_{p,i}$) for 3-BIDS and 15-BIDS is set to unity based in Figure 4 and Table 2, then a 3-fold decrease in Σ from the 11-BIDS monolayer should result in a 3-fold increase in the Cu(I)/Cu(II) ratio.

Because we contend that a conformational change of the 11-BIDS monolayer results a lower graft density, then to maintain an similar free radical concentration [P$^\bullet$], the ratio of activator to deactivator, Cu(I)/Cu(II), must be significantly higher from 11-BIDS than reactions from 3-BIDS or 15-BIDS. Table 2 shows that the relative ratio of [Cu(I)/Cu(II)] for the 11-BIDS monolayer is essentially 3 times larger than from 3-BIDS. Based on this analysis, the lower concentration of deactivator, Cu(II), should increase the lifetime of free radicals [P$^\bullet$], shifting the balance of the SI-ATRP activation/deactivation cycle to produce longer polystyrene graft polymer. This would help to explain why longer polystyrene graft polymers were grown from the 11-BIDS monolayers as shown in Figure 5. We conclude that on functionalized silica nanoparticles in anisole the conformation of the 11-BIDS initiator results in reduced availability of active bromine sites, dramatically reducing the polystyrene graft density during SI-ATRP.

## 4. Conclusions

The goal of this work was to quantify the impact of the alkoxysilane initiator carbon spacer length (CSL) on grafting polystyrene from silica nanoparticles with surface-initiated atom transfer radical polymerization (SI-ATRP) in anisole. To this end, three monoethoxysilane initiators were synthesized that varied in CSL from 3-, 11-, and 15-carbon repeat units. The initiators were termed 3-BIDS, 11-BIDS, and 15-BIDS, respectively, where the 15-BIDS initiator is a new molecule produced from this research. The attachment of the ATRP initiators to monodisperse silica nanoparticles (radius $R$ = 23 nm) was optimized in methyl isobutyl ketone (MIBK), a solvent in which the nanoparticles were electrostatically stable. The initiator site densities varied between 2.1 and 2.7 initiators/nm$^2$ with decreasing CSL, indicating that the silica nanoparticles were covered in a dense covalently attached monolayer of ATRP initiators.

The "grafting from" reactions were optimized to produce polystyrene graft polymers from the nanoparticle surfaces. Based on the results from GPC, DLS, and TGA, polystyrene of number-average molecular weight $M_n$ = 36 000 and 40 000 g/mol and of high graft density Σ = 0.7 chains/nm$^2$ were produced from the 3-BIDS and 15-BIDS monolayers. In contrast, a dramatic decrease in the PS graft density (Σ = 0.2 chains/nm$^2$) occurred when grafting PS from the 11-BIDS monolayer, which corresponded to a sizable increase in the graft polymer molecular weight $M_n$ = 24 000−88 000 g/mol. Inferring from the analysis of the polystyrene graft densities and the SI-ATRP reaction kinetics, a change in the conformation of the 11 CSL initiator is responsible for the reduced graft density and increased graft polymer molecular weight. Ultimately, our research indicates that discretion should be exhibited when using the 11-BIDS initiator as it could limit the polystyrene graft density, which may be useful when lower graft densities are desired.

**Acknowledgment.** This work was supported by the National Science Foundation (NSF) in the Division of Chemical, Bioengineering, Environment and Transport Systems (CBET-0649081).

**Supporting Information Available:** $^1$H NMR and $^{13}$C NMR scans of 3-BIDS, 11-BIDs, and 15-BIDS initiators along with a

representative TGA plot and DLS data. This material is available free of charge via the Internet at http://pubs.acs.org.

## References and Notes


(1) Behling, R. E.; Williams, B. A.; Staade, B. L.; Wolf, L. M.; Cochran, E. W. *Macromolecules* **2009**, *42*, 1867–1872.
(2) Bombalski, L.; Min, K.; Dong, H.; Tang, C.; Matyjaszewski, K. *Macromolecules* **2007**, *40*, 7429–7432.
(3) Pyun, J.; Jia, S.; Kowalewski, T.; Patterson, G. D.; Matyjaszewski, K. *Macromolecules* **2003**, *36*, 5094–5104.
(4) Von Werne, T.; Patten, T. E. *J. Am. Chem. Soc.* **2001**, *123*, 7497–7505.
(5) Kim, B. J.; Fredrickson, G. H.; Kramer, E. J. *Macromolecules* **2008**, *41*, 436–447.
(6) Garcia, A. J. *Adv. Polym. Sci.* **2006**, *203*, 171–190.
(7) Tsukagoshi, T.; Kondo, Y.; Yoshino, N. *Colloids Surf., B* **2007**, *54*, 101–107.
(8) Napier, M. E.; Desimone, J. M. *Polym. Rev.* **2007**, *47*, 321–327.
(9) Klein, J.; Kumacheva, E.; Mahalu, D.; Perahia, D.; Fetters, L. J. *Nature* **1994**, *370*, 634–636.
(10) Raviv, U.; Giasson, S.; Kampf, N.; Gohy, J. F.; Jerome, R.; Klein, J. *Nature* **2003**, *425*, 163–165.
(11) Landel, R. F.; Nielsen, L. E. *Mechanical Properties of Polymers and Nancomposites*, 2nd ed.; Marcel Dekker: New York, 1994.
(12) Tong, S. C. *Mater. Sci. Eng.* **2006**, *53*, 73–197.
(13) Bao, Z.; Bruening, M. L.; Baker, G. L. *Macromolecules* **2006**, *39*, 5251–5258.
(14) Dong, H.; Zhu, M.; Yoon, J. A.; Gao, H.; Jin, R.; Matyjaszewski, K. *J. Am. Chem. Soc.* **2008**, *130*, 12852–12853.
(15) Yang, Q.; Wang, L.; Xiang, W.; Zhou, J. F.; Tan, Q. H. *J. Polym. Sci., Polym. Chem.* **2007**, *45*, 3451–3459.
(16) Garcia, I.; Tercjak, A.; Zafeiropoulos, N. E.; Stamm, M.; Mondragon, I. *J. Polym. Sci., Polym. Chem.* **2007**, *45*, 4744–4750.
(17) Sun, Y.; Ding, X.; Zheng, Z.; Cheng, X.; Hu, X.; Peng, Y. *Eur. Polym. J.* **2007**, *43*, 762–772.
(18) Liu, Y. Z.; Chen, W. *Macromolecules* **2007**, *20*, 8881–8886.
(19) Carrot, G.; Diamanti, S.; Manuszak, M.; Charleux, B.; Vairon, J. P. *J. Polym. Sci., Polym. Chem.* **2001**, *39*, 4294–4301.
(20) Harrak, A. E.; Carrot, G.; Oberdisse, J.; Jestin, J.; Boue, F. *Macromol. Symp.* **2005**, *226*, 263–278.
(21) Ohno, K.; Morinaga, T.; Koh, K.; Tsujii, Y.; Fukuda, T. *Macromolecules* **2005**, *38*, 2137–2142.
(22) Radhakrishnan, B.; Ranjan, R.; Brittain, W. J. *Soft Matter* **2006**, *2*, 386–396.
(23) Savin, D. A.; Pyun, J.; Patterson, G. D.; Kowalewski, T.; Matyjaszewski, K. *J. Polym. Sci., Polym. Phys.* **2002**, *40*, 2667–2676.
(24) Wu, T.; Zhang, Y.; Wang, X.; Liu, S. *Chem. Mater.* **2008**, *20*, 101–109.
(25) Matyjaszewski, K.; Miller, P. J.; Shukla, N.; Immaraporn, B.; Gelman, A.; Luokala, B. B.; Siclovan, T. M.; Kickelbick, G.; Vallant, T.; Hoffmann, H.; Pakula, T. *Macromolecules* **1999**, *32*, 8716–8724.
(26) Yamamoto, S.; Ejaz, M.; Tsujii, Y.; Fukuda, T. *Macromolecules* **2000**, *33*, 5608–5612.
(27) Matyjaszewski, K.; Patten, T. E.; Xia, J. *J. Am. Chem. Soc.* **1997**, *119*, 674–680.
(28) Nanda, A. K.; Matyjaszewski, K. *Macromolecules* **2003**, *36*, 1487–1493.
(29) Patten, T. E.; Matyjaszewski, K. *Adv. Mater.* **1998**, *10*, 901–915.
(30) Xia, J.; Matyjaszewski, K. *Macromolecules* **1997**, *30*, 7697–7700.
(31) Wang, J. S.; Matyjaszewski, K. *J. Am. Chem. Soc.* **1995**, *117*, 5614–5615.
(32) Braunecker, W. A.; Matyjaszewski, K. *J. Mol. Catal. A: Chem.* **2006**, *254*, 155–164.
(33) Wang, Y.; Hu, S.; Brittain, W. J. *Macromolecules* **2006**, *39*, 5675–5678.
(34) Hiemenz, P. C.; Rajagopalan, R. *Principles of Colloid Science and Surface Chemistry*; Marcel Dekker: New York, 1997.
(35) Yanker, D. M.; Maurer, J. A. *Mol. Biosyst.* **2008**, *4*, 502–504.
(36) Battistella, M.; Cascione, M.; Fielder, B.; Wichmann, M. H. G.; Quaresimin, M.; Schulte, K. *Composites, Part A* **2008**, *39*, 1851–1858.
(37) Jana, S. C.; Jain, S. *Polymer* **2001**, *42*, 6897–6905.
(38) Bombalski, L.; Min, K.; Dong, H.; Tang, C.; Matyjaszewski, K. *Macromolecules* **2007**, *40*, 7429–7432.
(39) Wang, T.; Ou, C.; Yang, C. *J. Appl. Polym. Sci.* **2008**, *109*, 3421–3430.
(40) Zhou, L.; Yuan, J.; Hong, X. *Mater. Lett.* **2008**, *62*, 1372–1375.
(41) Jeyaprakash, J. D.; Samuel, S.; Ruhe, J. *Macromol. Rapid Commun.* **2002**, *23*, 277–281.
(42) Akgun, B.; Boyes, S. G.; Granville, A. M.; Brittain, W. J. *Polym. Prepr.* **2003**, *44*, 514–515.
(43) Jones, D. M.; Brown, A. A.; Huck, W. T. S. *Langmuir* **2002**, *18*, 1265–1269.
(44) Bogush, G. H.; Tracey, M. A.; Zukoski, C. F. *J. Non-Cryst. Solids* **1988**, *104*, 95–106.
(45) Stober, W.; Fink, A.; Bohn, E. *J. Colloid Interface Sci.* **1968**, *26*, 62–69.
(46) Rai, A. N.; Basu, A. *Org. Lett.* **2004**, *6*, 2861–2863.
(47) Suratwala, T. I.; Hanna, M. L.; Miller, E. L.; Whitman, P. K.; Thomas, I. M.; Ehrmann, P. R.; Maxwell, R. S.; Burnham, A. K. *J. Non-Cryst. Solids* **2003**, *316*, 349–363.
(48) Vansant, E. F.; Van Der Voot, P.; Vrancken, K. C. *Characterization and Chemical Modification of the Silica Surface*; Elsevier: Amsterdam, 1995.
(49) Sindorf, D. W.; Maciel, G. E. *J. Phys. Chem.* **1982**, *86*, 5208–5219.
(50) Tsujii, Y.; Ohno, K.; Yamamoto, S.; Goto, A.; Fukuda, T. *Adv. Polym. Sci.* **2006**, *197*, 1–45.
(51) Angelico, V. J.; Mitchell, S. A.; Wysocki, V. H. *Anal. Chem.* **2000**, *72*, 2603–2608.
(52) Nuzzo, R. G.; Dubois, L. H.; Allara, D. L. *J. Am. Chem. Soc.* **1990**, *112*, 558–569.
(53) Bryant, M. A.; Pemberton, J. E. *J. Am. Chem. Soc.* **1991**, *113*, 8284–8293.
(54) Bryant, M. A.; Pemberton, J. E. *J. Am. Chem. Soc.* **1991**, *113*, 3629–3637.
(55) Tao, F.; Bernasek, S. L. *Chem. Rev.* **2007**, *107*, 1408–1453.
(56) *Polymer Handbook*, 3rd ed.; Wiley-Interscience: New York, 1989.